A complex-valued first integral of Navier-Stokes equations: Unsteady Couette flow in a corrugated channel system

F. Marner, P. H. Gaskell, and M. Scholle

Citation: Journal of Mathematical Physics **58**, 043102 (2017); doi: 10.1063/1.4980086
View online: http://dx.doi.org/10.1063/1.4980086
View Table of Contents: http://aip.scitation.org/toc/jmp/58/4
Published by the American Institute of Physics

JOURNAL OF MATHEMATICAL PHYSICS **58**, 043102 (2017)

A complex-valued first integral of Navier-Stokes equations: Unsteady Couette flow in a corrugated channel system

F. Marner,[1] P. H. Gaskell,[1] and M. Scholle[2,a)]
[1]*School of Engineering and Computing Sciences, Durham University, Durham DH1 3LE, United Kingdom*
[2]*Institute for Automotive Technology and Mechatronics, Heilbronn University, D-74081 Heilbronn, Germany*

(Received 18 May 2016; accepted 30 March 2017; published online 19 April 2017)

For a two-dimensional incompressible viscous flow, a first integral of the governing equations of motion is constructed based on a reformulation of the unsteady Navier-Stokes equations in terms of complex variables and the subsequent introduction of a complex potential field; complementary solid and free surface boundary conditions are formulated. The methodology is used to solve the challenging problem of unsteady Couette flow between two sinusoidally varying corrugated rigid surfaces utilising two modelling approaches to highlight the versatility of the first integral. In the Stokes flow limit, the results obtained in the case of steady flow are found to be in excellent agreement with corresponding investigations in the open literature. Similarly, for unsteady flow, the results are in accord with related investigations, exploring material transfer between trapped eddies and the associated bulk flow, and vice versa. It is shown how the work relates to the classical complex variable method for solving the biharmonic problem and perspectives are provided as to how the first integral may be further utilised to investigate other fluid flow features. *Published by AIP Publishing.* [http://dx.doi.org/10.1063/1.4980086]

I. INTRODUCTION

In the first half of the 20th century, the complex variable method was developed for the solution of biharmonic problems in plane linear elasticity, which nowadays is considered a classical[1,2] approach. By combining the two Cartesian coordinates x and y to form the complex expression $\xi = x + \mathrm{i}y$, all solutions of the biharmonic equation $\Delta^2\psi = 0$ take the form

$$\psi = \Re\left[g_0(\xi) + \bar{\xi} g_1(\xi)\right], \tag{1}$$

with arbitrary holomorphic functions g_0 and g_1, the so-called *Goursat functions*; $\Re$ denotes the real part of the subsequent complex expression and $\bar{\xi} = x - \mathrm{i}y$ the complex conjugate of ξ. The problem is thus effectively reduced to one of finding two holomorphic functions in a domain Ω, boundary $\partial\Omega$, satisfying conditions which are typically of the form[1]

$$g_1(\xi) + \xi\overline{g_1'(\xi)} + \overline{g_0'(\xi)} = f(\xi), \quad \xi \in \partial\Omega. \tag{2}$$

One such approach is to represent g_0 and g_1 as Cauchy-type integrals of an unknown density function on the boundary, thus leading to the famous Sherman-Lauricella equation,[3] a Fredholm integral equation for the density which can be solved efficiently via a Nyström discretization in combination with fast multipole methods.[4] Other approaches are based on a direct expansion of the holomorphic functions as a Fourier series or on meromorphic functions with singularities outside of the domain, in which (2) is approximated via boundary element or collocation methods.[5–8] Although the biharmonic equation is not preserved under conformal transformation, diverse examples exist where

a)Electronic mail: markus.scholle@hs-heilbronn.de.

a mapping of the Goursat representation to computationally more convenient regions has proved useful.[1,9]

Beyond linear elasticity, complex variable methods have emerged as a wide-ranging and powerful tool in fluid mechanics,[8,10] where a variety of analytical solutions and computational methods have materialised, particularly for Stokes flow problems with free boundaries.[11–15] The benefits thereof stem from the mathematically important notion of the analyticity of the underlying holomorphic functions g_0 and g_1 which can be exploited for certain problems;[6,8] free surface boundary conditions, a notorious complicating feature, can be handled in the framework of the Goursat representation naturally due in the main to the complementary character of the stream function and Airy stress function.[16,17] Unfortunately, the method in its classical form is restricted to zero Reynolds number scenarios, i.e., to Stokes flow, in which the stream function remains biharmonic.

Of late, a *first integral* of Navier-Stokes equations has been constructed for two-dimensional steady flow:[18,19] by combining the u_x and u_y velocities in the form $u = u_x + \mathrm{i}u_y$ and by the subsequent introduction of an auxiliary potential field Φ fulfilling $p + \varrho\bar{u}u/2 + U = 4\partial^2\Phi/\partial\bar{\xi}\partial\xi$, an integrable equation of motion is obtained, ultimately leading to the following relationship:

$$\varrho\frac{u^2}{4} - \eta\frac{\partial u}{\partial\bar{\xi}} + 2\frac{\partial^2\Phi}{\partial\bar{\xi}^2} = 0\,. \tag{3}$$

By taking the derivative of Eq. (3) with respect to ξ, the Navier-Stokes equations are obtained in complex form. In a recent paper,[16] the close relationship between the first integral and the complex variable method has been shown: if a stream function Ψ is introduced according to

$$u = -2\mathrm{i}\frac{\partial\Psi}{\partial\bar{\xi}}\,, \tag{4}$$

it can be beneficially combined with the potential Φ to form the complex potential, $\chi = \Phi + \mathrm{i}\eta\Psi$, in terms of which the first integral (3) reads

$$\frac{\partial^2\chi}{\partial\bar{\xi}^2} = -\varrho\frac{u^2}{8}\,. \tag{5}$$

In the case of Stokes flow, the above equation reduces to

$$\frac{\partial^2\chi}{\partial\bar{\xi}^2} = 0\,, \tag{6}$$

which is a simple bianalytic equation, the solution of which is given by the combination $\chi = g_0(\xi) + \bar{\xi}g_1(\xi)$ of two holomorphic functions, as in (1). It is therefore justifiable to construe the first integral (5) to be a generalisation of the complex variable representation (6) towards viscous flows with inertia, with the difference that (5) no longer allows for a direct integration to the Goursat representation (1).

In what follows, a first integral is constructed for the more general case of unsteady flows: the derivation begins with a reformulation of the full two-dimensional Navier-Stokes equations in terms of complex variables prior to utilising the complex potential χ in order to achieve an integrable equation (Sec. II). It is shown how commonly encountered boundary conditions can be formulated in an elegant and useful form, where special attention is paid to prescribing those occurring at a free surface (Sec. III). In Section IV the new formulation is applied to the practically relevant problem of the unsteady Couette flow confined in a channel formed by two, horizontally aligned, corrugated surfaces, separated by a small distance. The upper surface is driven with a constant speed, while the lower one remains stationary. Attention is focussed on the effect of mass exchange between vortices residing in the valleys of the lower corrugated surface and the bulk flow. Finally, in Section V, perspectives as to the enhancement and future development of analytical and numerical methods for the investigation of viscous fluid flow problems, together with the issue of predicting the stability of film flows in particular, are provided.

II. FORMULATION OF THE FIELD EQUATIONS

A. Complex form of the Navier-Stokes equations for unsteady 2D flow

In two-dimensions, the Navier-Stokes equations and continuity equation governing an unsteady incompressible flow, assuming that the external force on the fluid is conservative with a given potential energy density $U(x, y)$, are

$$\varrho\left[\frac{\partial\vec{u}}{\partial t}+\vec{u}\cdot\nabla\vec{u}\right]=-\nabla p+\eta\Delta\vec{u}-\nabla U\,, \tag{7}$$

$$\nabla\cdot\vec{u}=0\,, \tag{8}$$

where $\vec{u}$ denotes the velocity field, p the pressure field, ϱ the mass density, and η the viscosity. Employing the complex variables ξ, $\overline{\xi}$ and the complex velocity field u, together with the stream function via (4), the Navier-Stokes equations (7) can be transformed into the following scalar complex PDE:

$$\frac{\partial}{\partial\overline{\xi}}\left[-\mathrm{i}\varrho\frac{\partial\Psi}{\partial t}+p+\varrho\frac{\bar{u}u}{2}+U\right]+\varrho\frac{\partial}{\partial\xi}\left(\frac{u^2}{2}\right)=2\eta\frac{\partial^2u}{\partial\overline{\xi}\partial\xi}\,, \tag{9}$$

while the continuity equation (8) is identically fulfilled by (4).

B. First integral using a complex potential of first order

By the introduction of a new complex potential M according to

$$-\mathrm{i}\varrho\frac{\partial\Psi}{\partial t}+p+\varrho\frac{\bar{u}u}{2}+U=2\frac{\partial M}{\partial\xi}\,, \tag{10}$$

an integrable form of Eq. (9),

$$\frac{\partial}{\partial\xi}\left[2\frac{\partial M}{\partial\overline{\xi}}+\varrho\frac{u^2}{2}-2\eta\frac{\partial u}{\partial\overline{\xi}}\right]=0\,, \tag{11}$$

is obtained which, following integration with respect to ξ, gives

$$2\frac{\partial M}{\partial\overline{\xi}}+\varrho\frac{u^2}{2}-2\eta\frac{\partial u}{\partial\overline{\xi}}=f(\overline{\xi})\,. \tag{12}$$

The function $f(\overline{\xi})$ on the right-hand side of the above equation can conveniently be set to zero by re-gauging the potential M according to

$$M\to M+\frac{1}{2}F(\overline{\xi}),\quad F'(\overline{\xi})=f(\overline{\xi}) \tag{13}$$

since the definition (10) allows M to be augmented by an arbitrary $\overline{\xi}$-dependent complex function. Utilising the stream function (4), Eq. (12) simplifies to

$$2\frac{\partial}{\partial\overline{\xi}}\left[M+2\mathrm{i}\eta\frac{\partial\Psi}{\partial\overline{\xi}}\right]+\varrho\frac{u^2}{2}=0\,. \tag{14}$$

C. Representation by a potential of second order

From a purely technical viewpoint, a first integral has been constructed successfully in the form (14) since by differentiation of the same with respect to ξ, the Navier-Stokes equations are recovered. That said, comparison with the first integral (5) for the case of steady flow does not reveal an obvious relationship between the two. However, this can be formally shown to be the case by introducing another complex potential χ fulfilling

$$M+2\mathrm{i}\eta\frac{\partial\Psi}{\partial\overline{\xi}}=2\frac{\partial\chi}{\partial\overline{\xi}}\,, \tag{15}$$

and leading directly to the compact form of the first integral Eq. (14),

$$4\frac{\partial^2\chi}{\partial\bar{\xi}^2}+\varrho\frac{u^2}{2}=0\,, \tag{16}$$

which matches the first integral (5) for steady flow perfectly. Surprisingly, there is no difference between the complex field equations whether the flow is steady or unsteady. Indeed, the unsteady character of the flow is apparent in the PDE (10) for the potential M, which after making use of (15) reads

$$-\mathrm{i}\left[\varrho\frac{\partial\Psi}{\partial t}-4\eta\frac{\partial^2\Psi}{\partial\bar{\xi}\partial\xi}\right]+p+\varrho\frac{\bar{u}u}{2}+U=4\frac{\partial^2\chi}{\partial\bar{\xi}\partial\xi}\,. \tag{17}$$

Accordingly, two complex equations for one complex potential χ, the real-valued stream function Ψ, and the pressure p are given via (16) and (17).

III. FORMULATION OF BOUNDARY CONDITIONS

Consider a simply connected domain with a boundary $x_i=f_i(s,t)$, parametrized with respect to the arc length s of the boundary. Furthermore, normal and tangential unit vectors along the boundary appear as

$$t_i(s,t)=f_i'(s,t)\,, \tag{18}$$

$$n_i(s,t)=\varepsilon_{ji}t_j(s,t)\,, \tag{19}$$

where ε_{ij} denotes the Levi-Civita symbol. In complex notation, the tangential vector is given as $f'(s,t)$ with $f(s,t)=f_1(s,t)+\mathrm{i}f_2(s,t)$ and $n=\mathrm{i}f'(s,t)$; note that $\bar{n}n=\bar{t}t=\bar{f}'f'=1$.

A. No-slip and no-penetration conditions at solid walls

In terms of the stream function Ψ, the no-slip and no-penetration conditions along a solid wall $\xi=f(s)$ at rest take the usual form,

$$\mathrm{Im}\left(f'\frac{\partial\Psi}{\partial\xi}\right)=0\,, \tag{20}$$

$$\Psi=\mathrm{const}\,, \tag{21}$$

of Dirichlet/Neumann boundary conditions.

B. Kinematic and dynamic boundary conditions at a free surface

In the case of a free surface $\xi=f(s,t)$, movement of the surface, given by $\dot{f}$, has to be considered. In general, the movement $\dot{f}$ and the flow velocity u at the surface are not identical, but their normal components are. Hence, their difference is strictly directed tangential to the surface, i.e., $u-\dot{f}=u_1f'$ with $u_1\in\mathbb{R}$, implying after multiplication with $\bar{f}'$ and taking the imaginary part that

$$u\bar{f}'-\bar{u}f'=\dot{f}\bar{f}'-\dot{\bar{f}}f'\,. \tag{22}$$

Equation (22) constitutes a kinematic boundary condition taking into account the coupling between the movement of the free surface and the flow velocity in the normal direction. Considering (4), this results in the following relationship:

$$\frac{\partial\Psi}{\partial s}=\frac{\mathrm{i}}{2}\left[\dot{f}\bar{f}'-\dot{\bar{f}}f'\right]=:\frac{\mathrm{i}}{2}\left\{f,\bar{f}\right\}\,, \tag{23}$$

where $\{\cdot,\cdot\}$ denotes the Poisson bracket of two functions.[20]

The dynamic boundary condition in its original form reads

$$\left[(p_0-p)\delta_{ij}+\eta\left(\frac{\partial u_i}{\partial x_j}+\frac{\partial u_j}{\partial x_i}\right)\right]_{x_k=f_k(s)}n_j=\sigma\frac{\partial t_i}{\partial s}\,, \tag{24}$$

with σ on the right-hand side denoting the surface tension and p_0 the ambient pressure. Transformation of (24) into complex representation provides the condition

$$(p_0 - p)n - 2\eta \mathrm{i}\frac{\partial u}{\partial \bar{\xi}}\bar{f}' = \sigma f'' , \tag{25}$$

at $\xi = f(s,t)$. Next, by multiplying Eq. (10) with n and Eq. (14) with $\bar{n}$, and evaluating them at $\xi = f(s,t)$, the sum of the two equations together with (25), after some manipulation, gives

$$\varrho\frac{\partial \Psi}{\partial t}f' - \varrho u\frac{\partial \Psi}{\partial s} + Un = \frac{\partial}{\partial s}\left[\sigma f' + 2\mathrm{i}M - \mathrm{i}p_0 f\right] \tag{26}$$

as the boundary condition for the complex potential M. The term $\mathrm{i}p_0 f$ can be eliminated by re-gauging the potential energy according to $U \to U - p_0$. By considering the kinematic boundary condition (23), the first two terms in Eq. (26) can be re-arranged as follows:

$$\begin{aligned}\frac{\partial \Psi}{\partial t}f' - u\frac{\partial \Psi}{\partial s} &= \frac{\partial \Psi}{\partial t}f' - \frac{\partial \Psi}{\partial \bar{\xi}}\left\{f,\bar{f}\right\} = \left[\frac{\partial \Psi}{\partial t} + \frac{\partial \Psi}{\partial \xi}f' + \frac{\partial \Psi}{\partial \bar{\xi}}\dot{\bar{f}}\right]f' - \frac{\partial \Psi}{\partial s}\dot{f} \\ &= \frac{\partial}{\partial t}\Psi\left(f,\bar{f},t\right)\frac{\partial f}{\partial s} - \frac{\partial}{\partial s}\Psi\left(f,\bar{f},t\right)\frac{\partial f}{\partial t} = \left\{\Psi(f,\bar{f},t),f\right\} .\end{aligned}$$

Finally, by choosing the representation (15) in terms of the complex potential χ, the dynamic boundary condition (26) can be re-written elegantly as

$$\varrho\left\{\Psi(f,\bar{f},t),f\right\} + Un = \frac{\partial}{\partial s}\left[\sigma f' + 4\mathrm{i}\frac{\partial}{\partial \bar{\xi}}(\chi - \mathrm{i}\eta\Psi)\right] . \tag{27}$$

For special flow conditions, for which the Poisson bracket in (27) vanishes (e.g., in the case of a steady flow) and the external force is time-independent, (27) becomes integrable; the associated first integral reads

$$\sigma f' + 4\mathrm{i}\frac{\partial}{\partial \bar{\xi}}(\chi - \mathrm{i}\eta\Psi) = \int Un\mathrm{d}s . \tag{28}$$

It is possible to reduce the above condition to a standard Dirichlet-Neumann form, which allows for an elegant numerical treatment; for details see Ref. 16.

Derivation of the field equations (16) and (17) in combination with boundary conditions of the form described in Sec. III represents a coherent extension of prior work on the integration of the incompressible Navier-Stokes equations.[16,18] In order to demonstrate the capabilities of this new approach and to focus on the distinguishing key feature, namely, its ability to handle challenging transient flows, the non-trivial problem of the Couette flow generated within an irregular flow geometry is considered below.

IV. UNSTEADY COUETTE FLOW CONFINED BETWEEN TWO CORRUGATED RIGID SURFACES

The case of the Couette flow for a Newtonian, incompressible fluid confined between two horizontally aligned rigid surfaces, both corrugated sinusoidally and driven by the movement of the upper surface with uniform velocity U_0, the lower one remaining stationary, is explored. The flow configuration is illustrated schematically in Fig. 1; the unsteady character of the flow being due to the geometry of the domain varying with time. The geometry is defined in terms of the mean film thickness H_0, the amplitudes A and H_1 of the lower and upper surfaces, respectively, and the wavelength λ for both surfaces. External forces are not considered subsequently.

Exploration of the above unsteady Couette problem ties in well with an existing series of experimental and numerical investigations on thin films and channel flows over periodically occurring topography,[15,21–23] which is a topic of considerable interest in diverse technical and industrial processes, for example, in coating[24] or lubrication[5,22,25] applications, heat exchangers, and evaporators.[26] The existence of isolated or periodically occurring topographical features as exemplified by the sinusoidal lower surface contour in Fig. 1 can give rise to the formation of closed eddy structures,[27–30]

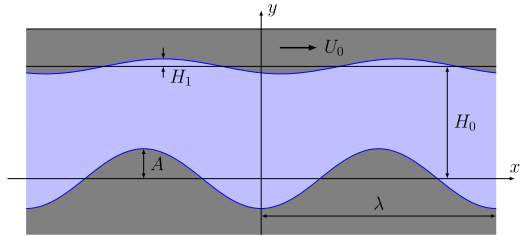

FIG. 1. Schematic of the unsteady Couette flow configuration, showing the relevant defining geometrical parameters.

leading to particle trapping and stagnant flow in separated flow regions. In the subsequent investigation the reader's attention is directed in particular to the inner flow structure present within the valleys of the lower surface topography and to the mechanism of mass exchange from the fluid in such valleys to the overlying flow and vice versa, as the channel thickness varies with time.

The effect of mass exchange together with the prospects of process enhancement have been studied by several authors: for instance, Wierschem and Aksel[27] observed experimentally the transport of inert tracers from the fluid in the valleys of sinusoidal topography in the presence of surface waves, enabled via a turnstile lobe mechanism; Horner *et al.*[31] provide a comprehensive overview of this mechanism for a modulated flow over a square cavity, while Wilson *et al.*[32] investigated, both experimentally and theoretically, the enhancement of transport and stirring between two rollers via lobe dynamics. Although these research topics are in the main associated with flows involving a free surface, the turnstile lobe effect is purely driven by temporal changes of the geometry of the flow domain, which can conveniently and more easily be studied in the model framework of the Couette flow, in which the geometry variance is artificially induced by specifying a non-uniform moving upper surface, that is, one with a well defined topography profile as shown in Fig. 1.

The boundary value problem as defined is formulated in (Sec. IV A) and the effect of mass exchange within the channel explored by means of two different self-contained methods, highlighting in addition different ways in which the new reformulation of the Navier-Stokes equations might be beneficially utilised. The first (Sec. IV B) is based on a generalised form of the Goursat representation (1), combined with a spectral Fourier discretization of the holomorphic functions involved; the second (Sec. IV C) is a finite element procedure based on a weak integral form of the field equations. The corresponding results are presented in Sec. IV D.

A. Equations of motion

All relevant quantities are scaled in terms of $\lambda/(2\pi)$, U_0, $\lambda/(2\pi U_0)$, and $2\pi\eta U_0/\lambda$ for lengths, velocities, the time, and for pressure, respectively. Consequently, the set of relevant parameters is reduced to two non-dimensional amplitudes a, h_1, a non-dimensional film thickness h_0 and the Reynolds number Re given by

$$\mathrm{Re} := \frac{\varrho U_0 \lambda}{2\pi\eta}, \qquad a := \frac{2\pi A}{\lambda}, \qquad h_0 := \frac{2\pi H_0}{\lambda}, \qquad h_1 := \frac{2\pi H_1}{\lambda}. \tag{29}$$

Accordingly, the scaled governing field equations (16) and (17) read

$$-\mathrm{Re}\frac{u^2}{2} = 4\frac{\partial^2 \chi}{\partial \bar{\xi}^2}, \tag{30}$$

$$-\mathrm{i}\left[\mathrm{Re}\frac{\partial \Psi}{\partial t} - 4\frac{\partial^2 \Psi}{\partial \bar{\xi}\partial \xi}\right] + p + \mathrm{Re}\frac{\bar{u}u}{2} = 4\frac{\partial^2 \chi}{\partial \bar{\xi}\partial \xi}. \tag{31}$$

The two boundaries formed by the lower $\xi = \beta(x)$ and upper $\xi = \varphi(x,t)$ corrugated surfaces are given by the functions

$$\beta(x) := x - \mathrm{i}a\cos x, \tag{32}$$

$$\varphi(x,t) := x + \mathrm{i}h_0 - \mathrm{i}h_1\cos(x-t), \tag{33}$$

along which the following no-slip/no-penetration conditions have to be fulfilled,

$$u\left(\beta(x),\bar{\beta}(x),t\right)=0\,, \tag{34}$$

$$u\left(\varphi(x,t),\bar{\varphi}(x,t),t\right)=1\,. \tag{35}$$

As an initial condition the fluid is assumed to be at rest, that is,

$$\Psi\left(\xi,\bar{\xi},t_0\right)=\chi\left(\xi,\bar{\xi},t_0\right)=0\,. \tag{36}$$

With reference to the work of Scholle *et al.*[25] and Esquivelzeta-Rabell *et al.*,[33] who have shown for the steady Couette flow generated with a flat upper driving surface that inertial effects play a minor role only up to Reynolds numbers with a value of about 10, by restricting the current investigation to Reynolds number $\mathrm{Re}\leq 10$ the nonlinear terms in the governing field equations (30) and (31) can be effectively omitted while retaining the Reynolds number in the term involving the time derivative, leading to

$$p-\mathrm{i}\left[\mathrm{Re}\frac{\partial\Psi}{\partial t}-4\frac{\partial^2\Psi}{\partial\bar{\xi}\partial\xi}\right]=4\frac{\partial^2\chi}{\partial\bar{\xi}\partial\xi}\,, \tag{37}$$

$$\frac{\partial^2\chi}{\partial\bar{\xi}^2}=0\,. \tag{38}$$

Below, variants of the time-dependent Couette flow, involving aspect ratios of $a<h_0<2\pi$ and $h_1\ll a$, are considered.

B. Asymptotic model and method of solution

1. Generalised Goursat form

According to earlier studies,[5,34] the stream function for the case of steady Stokes flow with $h_1=0$ can conveniently be written as

$$\Psi_{\mathrm{s}}=By^2+2\Re\left[R(\xi)+yQ(\xi)\right]\,, \tag{39}$$

where the constant B and the two 2π-periodic holomorphic functions R and Q are determined by the boundary conditions. By identifying $g_0(\xi)=2R(\xi)-\mathrm{i}\xi Q(\xi)-B\xi^2/2$ and $g_1(\xi)=\mathrm{i}Q(\xi)+B\xi/2$, it becomes obvious that (39) is a variant of the Goursat form (1), by which it is guaranteed that Ψ_{s} fulfils the biharmonic equation, $\Delta^2\Psi_{\mathrm{s}}=0$.

The stream function Ψ for the unsteady flow with $h_1>0$ is expected to differ from (39). However, neglecting inertia and assuming small Reynolds numbers, $\mathrm{Re}<1$, it is proven, see Appendix A, that $\Delta^3\Psi=\mathcal{O}\left(\mathrm{Re}^2\right)$, motivating the following analytical "triharmonic" form for Ψ,

$$\Psi=By^2+2\Re\left[R(\xi,t)+yQ(\xi,t)+\mathrm{Re}\frac{y^2}{2}P(\xi,t)\right]\,, \tag{40}$$

which is obviously a generalisation of (39) containing a third 2π-periodic holomorphic function P and considering time-dependence for the three functions P, Q, R and the parameter B. The analytical form $\partial\chi/\partial\bar{\xi}=f(\xi,t)$ is obtained directly from (38). Inserting this and (40) into the field equation (37) and neglecting terms of order $\mathcal{O}\left(\mathrm{Re}^2\right)$, the following identity is implied for the pressure field:

$$p=4f'-2\mathrm{i}B-\mathrm{i}\Im\left\{-4Q'-\mathrm{Re}\left[2\mathrm{i}\left(\dot{R}-P\right)+2y\left(\mathrm{i}\dot{Q}+2P'\right)\right]\right\}\,, \tag{41}$$

where the prime denotes a derivative with respect to ξ. Since the pressure has to be real-valued, the first three terms $4f'-2\mathrm{i}B-\mathrm{i}\dot{B}y^2$ equate to the complex expression inside the curly parentheses, leading to

$$4f'=2\mathrm{i}B-4Q'-\mathrm{Re}\left[2\mathrm{i}\left(\dot{R}-P\right)+2y\left(\mathrm{i}\dot{Q}+2P'\right)\right]+p_0(t)\,. \tag{42}$$

By taking the derivative of the above equation with respect to $\bar{\xi}$ and considering $\partial y/\partial\bar{\xi}=\mathrm{i}/2$, the identity

$$\mathrm{i}\dot{Q}+2P'=0 \tag{43}$$

is obtained, revealing that the two complex functions P and Q take the form of a PDE.

2. Boundary conditions

a. Perturbation approach. According to the aforementioned restriction $h_1 \ll 1$, the decomposition

$$Q(\xi,t) = Q_\mathrm{s}(\xi) + h_1 Q_\mathrm{u}(\xi,t)\,, \tag{44}$$

$$R(\xi,t) = R_\mathrm{s}(\xi) + h_1 R_\mathrm{u}(\xi,t)\,, \tag{45}$$

$$P(\xi,t) = h_1 P_\mathrm{u}(\xi,t) \tag{46}$$

of the three complex functions P, Q, R is applied, where the subscript "s" denotes the corresponding steady flow ($h_1 = 0$) and "u" the small perturbation invoked by the moving, slightly corrugated, upper surface. As a consequence, the complex conjugate of the complex velocity field is likewise decomposed as $\bar{u} = 2\mathrm{i}\partial\Psi/\partial\xi = \bar{u}_\mathrm{s} + h_1\bar{u}_\mathrm{u}$ with

$$\bar{u}_\mathrm{s} := 2By + 2\mathrm{i}\left[R_\mathrm{s}' + yQ_\mathrm{s}'\right] + 2\Re Q_\mathrm{s}\,, \tag{47}$$

$$\bar{u}_\mathrm{u} := 2\mathrm{i}\left[R_\mathrm{u}' + yQ_\mathrm{u}'\right] + \mathrm{Re}\frac{y^2}{2}\dot{Q}_\mathrm{u} + 2\Re\left[Q_\mathrm{u} + \mathrm{Re}\, yP_\mathrm{u}\right]\,. \tag{48}$$

Considering the above, the complex conjugate of the no-slip/no-penetration condition (34) at the lower surface can be decomposed into the two boundary conditions,

$$\bar{u}_\mathrm{s}\left(\beta(x), \bar{\beta}(x)\right) = 0\,, \tag{49}$$

$$\bar{u}_\mathrm{u}\left(\beta(x), \bar{\beta}(x), t\right) = 0\,, \tag{50}$$

while at the upper surface a domain perturbation is given by (33) due to h_1 appearing explicitly. Via a Taylor expansion of the no-slip/no-penetration condition (35) with respect to h_1 and sorting terms by powers of h_1, one ends up with the two conditions,

$$\bar{u}_\mathrm{s}\left(x + \mathrm{i}h_0, x - \mathrm{i}h_0\right) = 1\,, \tag{51}$$

$$\bar{u}_\mathrm{u}\left(x + \mathrm{i}h_0, x - \mathrm{i}h_0, t\right) = \mathrm{i}\left[\frac{\partial\bar{u}_\mathrm{s}}{\partial\xi} - \frac{\partial\bar{u}_\mathrm{s}}{\partial\bar{\xi}}\right]\cos(x-t)\,. \tag{52}$$

With reference to Appendix B, these two equations reveal a hierarchy: the inhomogeneity in Equation (52) for the first order perturbation depends on the base solution. Apart from this, the inhomogeneity is purely harmonic with respect to time. Due to the linearity of the problem, the perturbation must be harmonic with respect to time too, implying the following analytical form:

$$P_\mathrm{u}(\xi,t) = p^+(\xi)\exp(\mathrm{i}t) + p^-(\xi)\exp(-\mathrm{i}t)\,, \tag{53}$$

$$Q_\mathrm{u}(\xi,t) = q^+(\xi)\exp(\mathrm{i}t) + q^-(\xi)\exp(-\mathrm{i}t)\,, \tag{54}$$

$$R_\mathrm{u}(\xi,t) = r^+(\xi)\exp(\mathrm{i}t) + r^-(\xi)\exp(-\mathrm{i}t) \tag{55}$$

for the three holomorphic functions. By inserting the above forms into Eq. (43), it follows that

$$2p^{\pm'}(\xi) = \pm q^\pm(\xi)\,. \tag{56}$$

b. Discretization by Fourier decomposition. In line with the work of others,[5,22] the periodic holomorphic functions are represented by a truncated Fourier series as follows:

$$Q_\mathrm{s}(\xi) = \sum_{k=-N}^{N} Q_k \exp(\mathrm{i}k\xi)\,, \qquad q^\pm(\xi) = \sum_{k=-N}^{N} q_k^\pm \exp(\mathrm{i}k\xi)\,, \tag{57}$$

$$R_\mathrm{s}(\xi) = \sum_{k=-N}^{N} R_k \exp(\mathrm{i}k\xi)\,, \qquad r^\pm(\xi) = \sum_{k=-N}^{N} r_k^\pm \exp(\mathrm{i}k\xi)\,, \tag{58}$$

up to order $N \in \mathbb{N}$, reducing the problem to a finite set of complex coefficients and the yet unknown constant B. For the two remaining functions $p^{\pm}(\xi)$, Equation (56) are fulfilled identically by

$$p^{\pm}(\xi) = p_0 \mp \mathrm{i} \sum_{\substack{k=-N \\ k\neq 0}}^{N} \frac{q_k^{\pm}}{2k} \exp(\mathrm{i}k\xi)\,, \tag{59}$$

with integration constant p_0. On inserting the above series representation (57)–(59) into boundary conditions (49)–(52), a linear set of algebraic equations for the coefficients $Q_k, R_k, q_k^{\pm}, r_k^{\pm}, p_0$ and B is obtained. Full details regarding the formulation of this algebraic set of equations are provided in Appendix B.

C. Numerical model and method of solution

The starting point for a weak integral formulation is again the linear field equations (37) and (38). As the pressure is not of relevance for the problem under investigation, the imaginary part only of (37) is taken into account, namely,

$$\frac{\mathrm{Re}}{4}\frac{\partial \Psi}{\partial t} - \frac{\partial^2 \Psi}{\partial \bar{\xi}\partial \xi} = -\mathrm{Im}\left(\frac{\partial^2 \chi}{\partial \bar{\xi}\partial \xi}\right) =: -\Phi(\xi, \bar{\xi}, t)\,, \tag{60}$$

and from (38) it follows directly that

$$\mathrm{Im}\left(\frac{\partial^4 \chi}{\partial \bar{\xi}^2 \partial \xi^2}\right) = \frac{\partial^2 \Phi}{\partial \bar{\xi}\partial \xi} = 0\,, \tag{61}$$

in which the more convenient real-valued field Φ has been introduced, thus replacing the complex-valued χ.

In order to solve for the modified field equations (60) and (61), complemented by the conditions (34)–(36), the implicit Crank-Nicolson time discretization scheme is combined with a weak Galerkin finite element formulation, resulting in a second order accurate method in both space and time. Consequently, iteration in time, starting with $\Psi_0 = \Phi_0 = 0$, is accomplished according to

$$\frac{\mathrm{Re}}{2\Delta t}\Psi_{t+1} - \frac{\partial^2 \Psi_{t+1}}{\partial \bar{\xi}\partial \xi} + \Phi_{t+1} = \frac{\mathrm{Re}}{2\Delta t}\Psi_t + \frac{\partial^2 \Psi_t}{\partial \bar{\xi}\partial \xi} - \Phi_t\,, \tag{62}$$

$$\frac{\partial^2 \Phi_{t+1}}{\partial \bar{\xi}\partial \xi} = 0\,, \tag{63}$$

and at each time step a spatial FEM problem is solved based on the weak variational formulation:

Find $\Psi \in \left\{\Psi \in H^1(\Omega) \,\middle|\, \Psi = g_1, \frac{\partial \Psi}{\partial n} = g_2 \text{ on } \partial\Omega\right\}$ and $\Phi \in H^1(\Omega)$, such that for all $v \in H^1(\Omega)$ and $w \in H_0^1(\Omega)$,

$$\frac{\mathrm{Re}}{2\Delta t}\langle \Psi_{t+1}, v\rangle_{L_2,\Omega} - \langle \nabla\Psi_{t+1}, \nabla v\rangle_{L_2,\Omega} + \langle \Phi_{t+1}, v\rangle_{L_2,\Omega} = \langle g_2, v\rangle_{L_2,\partial\Omega} + b_{t+1}(v, \Psi_t)\,, \tag{64}$$

$$b_0 = 0\,, \quad b_{t+1}(v, \Psi_t) = \frac{\mathrm{Re}}{\Delta t}\langle \Psi_t, v\rangle_{L_2,\Omega} - b_t\,, \tag{65}$$

$$\langle \nabla\Phi_{t+1}, \nabla w\rangle_{L_2,\Omega} = 0\,, \tag{66}$$

in which the standard L_2-inner product is used and the standard Sobolev space

$$H^1(\Omega) = \{v \in L^2(\Omega) : D^{\alpha} v \in L^2(\Omega)\ \forall |\alpha| \leq 1\}\,, \tag{67}$$

consisting of square-integrable functions with weak first order derivatives again in L_2; H_0^1 comprises H^1-functions with zero boundary conditions. Ω and $\partial\Omega$ denote the computational domain and its boundary, respectively; the functions g_1 and g_2 define the space and time-dependent velocity boundary conditions for the stream function.

In order to provide a complete description of the solution procedure, it is necessary to take a closer look at the boundary conditions. First of all, the no-slip and no-penetration conditions at the lower,

stationary surface lead to $g_1(x, \beta(x), t) = g_2(x, \beta(x), t) = 0$, in which the arbitrary constant offset of the stream function is fixed. The periodicity of the domain is incorporated simply by identifying the related nodes on the left and right-hand side of the finite element grid; therefore a separate periodic boundary treatment can be omitted. In order to avoid complications with the upper moving bounding surface and any time-dependent re-meshing issues, condition (33) and (35) is approximated as a flat surface with a constant height of $h_0 - h_1$, which is directly *beneath* the surface waviness. In this sense, the impact of the lower surface corrugations on the flow near the upper surface is neglected so that for the approximation of Ψ close to the height $h_0 - h_1$, a geometry with $\tilde{h}_0 = h_0$, $\tilde{h}_1 = h_1$ and $\tilde{a} = 0$ is assumed.

An analytical approximation of the above reference problem can be derived under the assumptions of lubrication theory and for moderate aspect ratios,[5] giving

$$\Psi(x, h_0 - h_1, t) \approx U_0 y - \Psi_0(x - t, h_0 - h_1) + c_0\,, \tag{68}$$

$$\Psi_0(x, y) = \frac{h_0(h_0^2 - h_1^2)}{2h_0^2 + h_1^2} Y^2(3 - 2Y) - h_0 Y^2(1 - Y)\left(1 + \frac{h_1}{h_0}\cos(x)\right), \tag{69}$$

$$Y(x, y) := \frac{y + h_1\cos(x)}{h_0 + h_1\cos(x)}\,. \tag{70}$$

The boundary functions g_1 and g_2 can than be derived from (68) and its normal derivative. In order to fix the remaining constant c_0, note that an additional constraint for the vorticity ω is assigned to the upper plate as is similarly the case for all multiply connected domains.[35] Denoting the upper boundary as Γ_u and the tangential and normal velocity components with subscripts τ and n, respectively, then by integrating the equation:

$$\mathrm{Re}\left[\frac{\partial u_\tau}{\partial t} + u_\tau\frac{\partial u_\tau}{\partial \tau}\right] = -\frac{\partial p}{\partial \tau} + \frac{\partial \omega}{\partial n}\,, \tag{71}$$

over Γ_u, the condition:

$$-\frac{1}{\mathrm{Re}}\int_{\Gamma_u}\frac{\partial \omega}{\partial n}\,\mathrm{d}\Gamma_u = \frac{\partial u_\tau}{\partial t}\int_{\Gamma_u}\mathrm{d}\Gamma_u + \int_{\Gamma_u}\frac{\partial}{\partial \tau}\left[\frac{1}{2}u_\tau^2 + p\right]\mathrm{d}\Gamma_u = 0 \tag{72}$$

is established, which in the present context translates as the following condition on the potential Φ:

$$0 = \int_{\Gamma_u}\frac{\partial \omega}{\partial n}\,\mathrm{d}\Gamma_u = \int_{\Gamma_u}\frac{\partial}{\partial n}\left[\frac{\mathrm{Re}}{4}\frac{\partial \Psi}{\partial t} + \Phi\right]\mathrm{d}\Gamma_u = \int_{\Gamma_u}\frac{\partial \Phi}{\partial n}\,\mathrm{d}\Gamma_u\,. \tag{73}$$

D. Results and discussion

1. Asymptotic results

a. Steady stokes flow. According to Appendix B 1, the original set of $4N + 3$ algebraic equations is reduced to the set (B6) of $2N + 1$ equations for the coefficients $Q_n, R_n; n > 0$ and Q_0. This set of equations was solved for $a = \pi/8$ and $h_0 = \pi/4$ using Maple at a truncation order of $N = 24$. The remaining coefficients are determined according to (B3), (B4),and (B2). A plot of the resulting streamline pattern is shown in Fig. 2: note that the presence of a closed eddy in the valley formed by the lower surface topography is in complete accordance with prior results reported in the literature.[5,22,25,34]

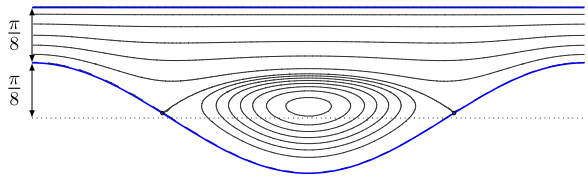

FIG. 2. Steady Couette flow ($h_1 = 0$) for $a = \pi/8$ and $h_0 = \pi/4$, $\mathrm{Re} = 0$: streamlines revealing the associated flow structure. Stationary points are indicated by a bold dot.

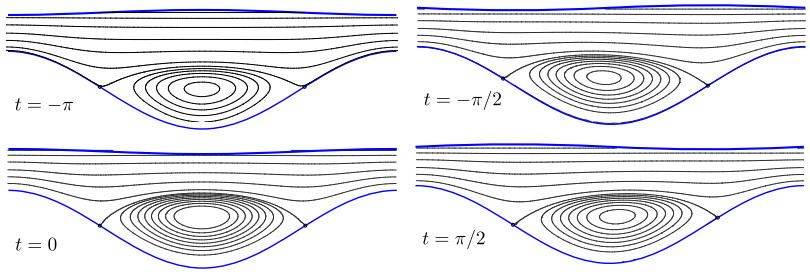

FIG. 3. Unsteady Couette flow with $a = \pi/8$, $h_0 = \pi/4$, Re = 0.5, and $h_1 = 0.02$; instantaneous streamline patterns, at four different times, revealing the associated flow structure.

b. Unsteady non-Stokes flow. The coefficients $q_k^{\pm}$ and $r_k^{\pm}$, by which the complex functions for the first perturbation order are determined, result from solving the set of equations (B7) and (B9) given in Appendix B 2. Again, Maple is used to solve the associated algebraic equation set. Since the perturbation provides a small contribution only to the entire solution, a truncation order of $N = 12$ proves sufficiently accurate.

As for the steady Stokes flow case, the same geometric parameters are chosen for $a = \pi/8$ and $h_0 = \pi/4$; the additional parameter for unsteady flow, the choice being Re = 0.5 and thus $h_1 = 0.02$. The resulting instantaneous streamline patterns at four different times, $t \in \{-\pi, -\pi/2, 0, \pi/2\}$, are shown in Fig. 3: the time-dependence of the flow invoked by the corrugated upper surface is considerable, especially regarding the shape and skewness of the eddy, regardless of the small amplitude h_1. Since during each time period the eddy occupies slightly different regions of the flow domain, it is only to be expected that some fluid particles are located in the vicinity of the border between the eddy and main flow, while those trapped inside (outside) of the eddy at some point in time will be located outside (inside) the eddy at some different point in time due to an associated shift of the separating streamline, or separatrix. Accordingly, the mechanism for material exchange between an eddy and the main flow is captured qualitatively. In order to study this feature in more detail, the movement of material particles has to be visualised by path lines or sweep lines. This is conveniently performed numerically as described below.

2. Numerical results

FEM calculations based on the weak formulation (64)–(66) were performed within a Matlab framework, with a triangular mesh structure containing of the order of 40 thousand elements and employing quadratic Lagrange elements for all test and solution spaces; one time period, $T = \lambda/U_0$, is discretized over 150 time steps.

First a representative example geometric configuration with $\lambda = 2\pi$, $a = \pi/4$, $h_0 = \pi$, and $h_1 = a/20$, for a Reynolds number of Re = 10, is considered. Figure 4(a) shows that a time periodic flow field is established after just two time periods and that in this time-periodic regime the size and the shape of the eddy lie on either side of the equivalent steady state configuration which exists when $h_1 = 0$, see Fig. 4(b). In this context the question arises whether particles entrapped within the steady-state eddy can be made to escape by being flushed away by the bulk flow. The subsequent investigations indicate that in general a mass exchange, at least in both directions, cannot be expected for arbitrarily small amplitudes h_1 of the upper plate. To visualise material transport, the time evolution of sweep lines was computed, i.e., material lines consisting of the same fluid particles at all times, their initial shape being conveniently defined by corresponding streamlines at a particular time.

Figure 5 shows results for the above geometry in more detail, in the form of a sequence of snap-shots. At the time $t = 0$ the corrugated upper surface is considered to instantaneously accelerate to a velocity of U_0 and then the flow is subsequently solved for over 20 time periods; the direction of flow is always from left to right. At $t = 3.44\,T$, representing a state with a maximum

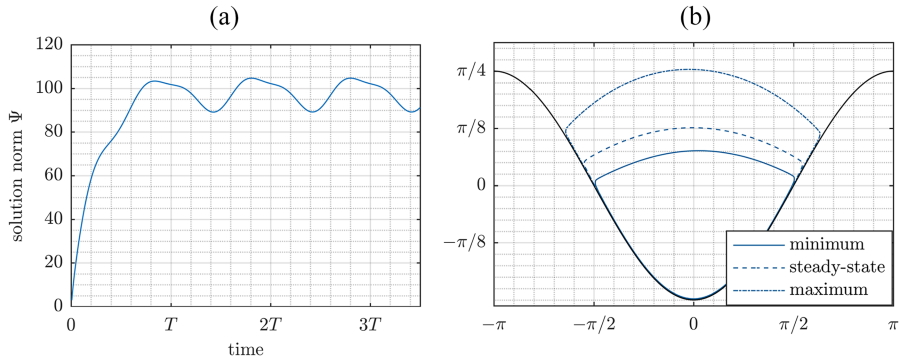

FIG. 4. Couette flow between corrugated surfaces for the case of $\lambda = 2\pi$, $a = \pi/4$, $h_0 = \pi$, and $h_1 = a/20$ with a Reynolds number Re = 10. (a) Euclidean norm of the FEM solution vector of Ψ evolving with time; a time-periodic flow is established after a $2T$ time period. (b) Separatrices confining the eddy region from the bulk flow for three different states; these being the minimum and maximum eddy shape in terms of surface area occurring in the time-periodic regime as well as the steady-state eddy shape corresponding to the case of $h_1 = 0$.

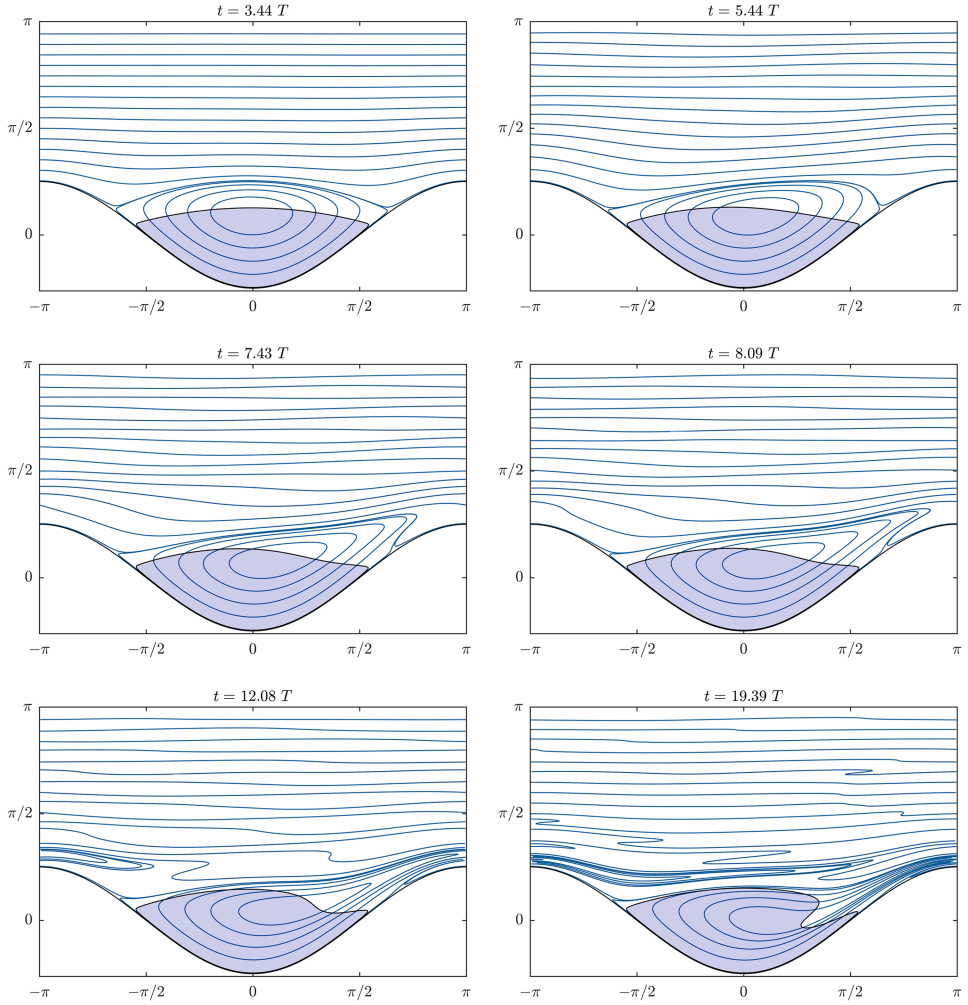

FIG. 5. Sweep lines at different times for the case: $a = \pi/4$, $h_0 = \pi$, $h_1 = a/20$, and Re = 10; six snap-shot solutions obtained over 20 time periods. The initial shape of the sweep lines at a state with a maximum eddy size ($t = 3.44\,T$) corresponds to the instantaneous streamline pattern; the shaded area represents the material time evolution of the area defined at $t = 3.44\,T$ from the eddy shape of the corresponding steady-state flow.

eddy size, the instantaneous streamline pattern is captured in terms of the "initial" sweep lines present, the *material movement* of which is tracked in the following sequence of plots, obtained by solving the advection equation $\frac{\mathrm{d}x}{\mathrm{d}t} = u(x,t)$ for the trajectories $x(t)$ via a fourth-order Runge-Kutta scheme; each sweep line is represented by between 500 and 1000 fluid particles. Moreover, the shaded area represents the material time evolution of the fluid region which at time $t = 3.44\,T$ is initially defined by the *shape of the original closed steady-state eddy*. From the deformation of the sweep lines, it can be seen that material from the maximum eddy is flushed away with the bulk flow and fluid in the region of its bounding separatrix plunges lower down the right hand side of the valley to displace the separatrix bounding the shaded former steady-state area. Part of the fluid originally in the maximum eddy is entrained into the shaded region; however, over the course of solution the material within the steady state eddy region is not expelled and remains trapped. These observations clearly indicate that small perturbations of the steady-state flow, interpreted as being due to the corrugations in the upper plate, leave the material movement of the steady-state flow qualitatively invariant: a certain amount of fluid particles covering an area smaller than the maximum eddy size but larger than the minimum eddy size, as expected fairly close to the shape of the steady-state eddy, remain trapped; whereas fluid particles above this region are flushed away.

In contrast to the above, the following example considers the effect of varying the amplitude of the upper plate h_1. Figures 6–8 show sweep lines for the configuration $\lambda = 2\pi$, $a = \pi/8$, $h_0 = \pi/4$, $\mathrm{Re} = 1$ with different amplitudes $h_1 = 0.01$, $h_1 = 0.03$, and $h_1 = 0.09$. As before, several time

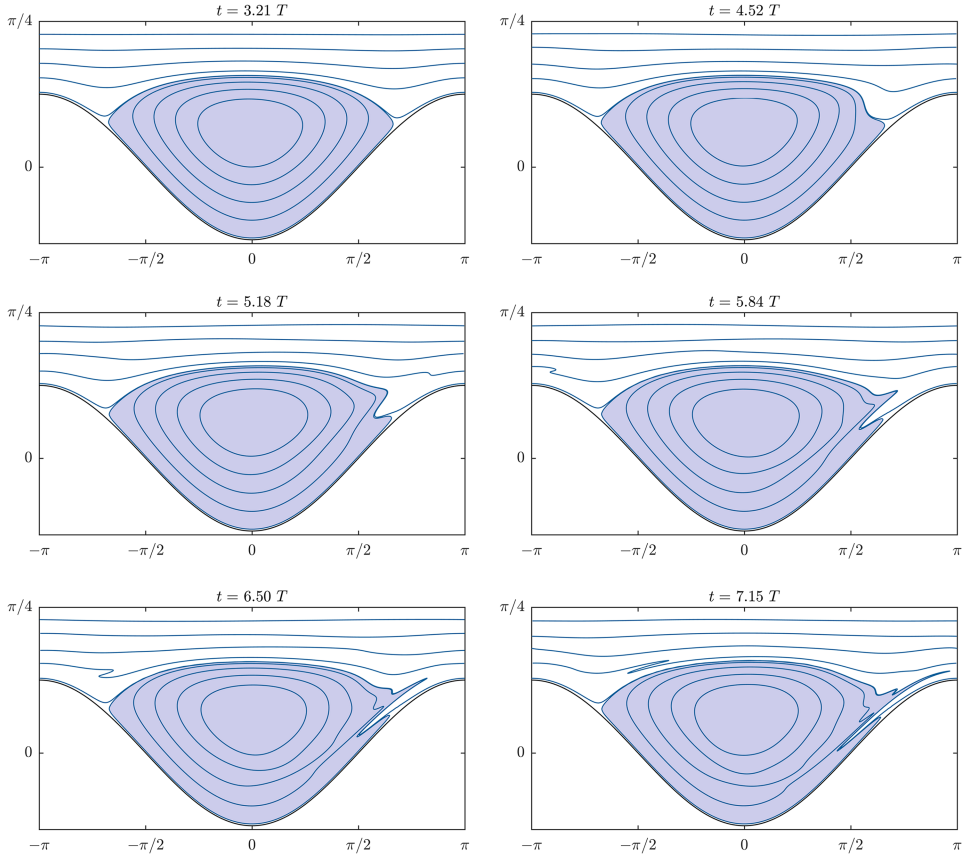

FIG. 6. Sweep lines at different times for the case: $h_0 = \pi/4$, $a = \pi/8$, $h_1 = 0.01$, $\mathrm{Re} = 1$; the shaded area represents the particle distribution at successive times, that was initially confined within the steady-state closed eddy (upper, top left-hand image) at the onset of the unsteady behaviour. Mass transfer takes place between the eddy region and the bulk flow and vice versa.

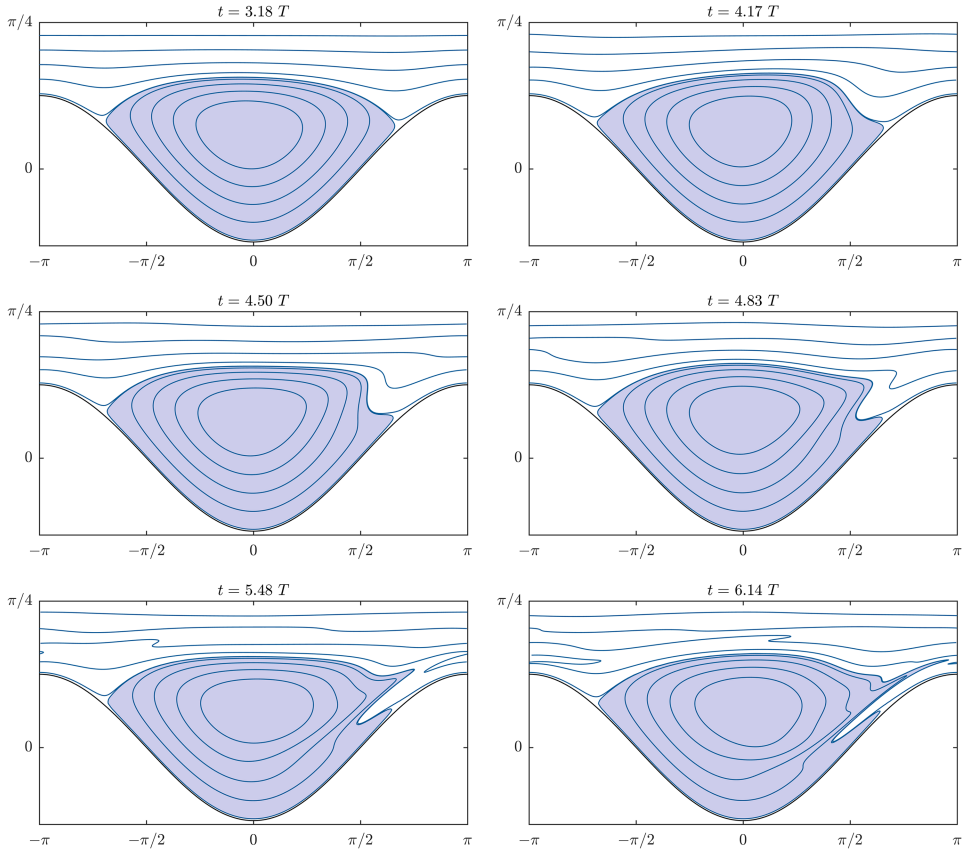

FIG. 7. Sweep lines at different times for the case: $h_0 = \pi/4$, $a = \pi/8$, $h_1 = 0.03$, $\mathrm{Re} = 1$; the shaded area represents the particle distribution at successive times, that was initially confined within the steady-state closed eddy (upper, top left-hand image) at the onset of the unsteady behaviour. Mass transfer takes place between the eddy region and the bulk flow and vice versa.

periods are allowed to pass before the flow can be considered to lie in the time-periodic regime; in this case the streamlines are captured at times when the eddy shape is closest to the steady state case $h_1 = 0$, this being the reason for the slightly different starting times for the three computations shown. The time-dependent variation of channel thickness leads to periodically increasing and decreasing eddy formation in the valley of the corrugated lower surface. As the solution proceeds, material from within the initially closed eddy region is exchanged with the bulk flow, as the separatrix detaches from the right-hand side of the valley and fluid is entrained into the valley; at the same time fluid is ejected from the eddy into the bulk flow. In all three cases material exchange takes place in both directions, from the bulk flow to the eddy region and vice versa. For the case $h_1 = 0.01$ the effect appears marginal, while for increasing amplitude h_1 the amount of material exchange grows significantly. The above results exhibit a variant of the "turnstile lobe effect," as observed for instance by Wierschem and Aksel[27] and Horner *et al.*,[31] and therefore represent a qualitative difference to the case of Fig. 5. This leads to the assumption that the amount of mass exchange between the steady-state eddy and the bulk flow depends proportionally, involving a geometry-dependent constant, on the energy induced by the perturbation signal, e.g., by the corrugation of the upper surface, while a certain minimum energy is necessary to initiate the process at all. Revealing in this context would certainly be the study of different upper corrugated surface wavelengths in relation to the lower surface contour. Furthermore, for the small Reynolds numbers considered in this example, i.e., $\mathrm{Re} \leq 10$, the influence of the nonlinear terms that have been effectively neglected is anticipated to increase slightly any effects due to a more pronounced asymmetry of the eddy.

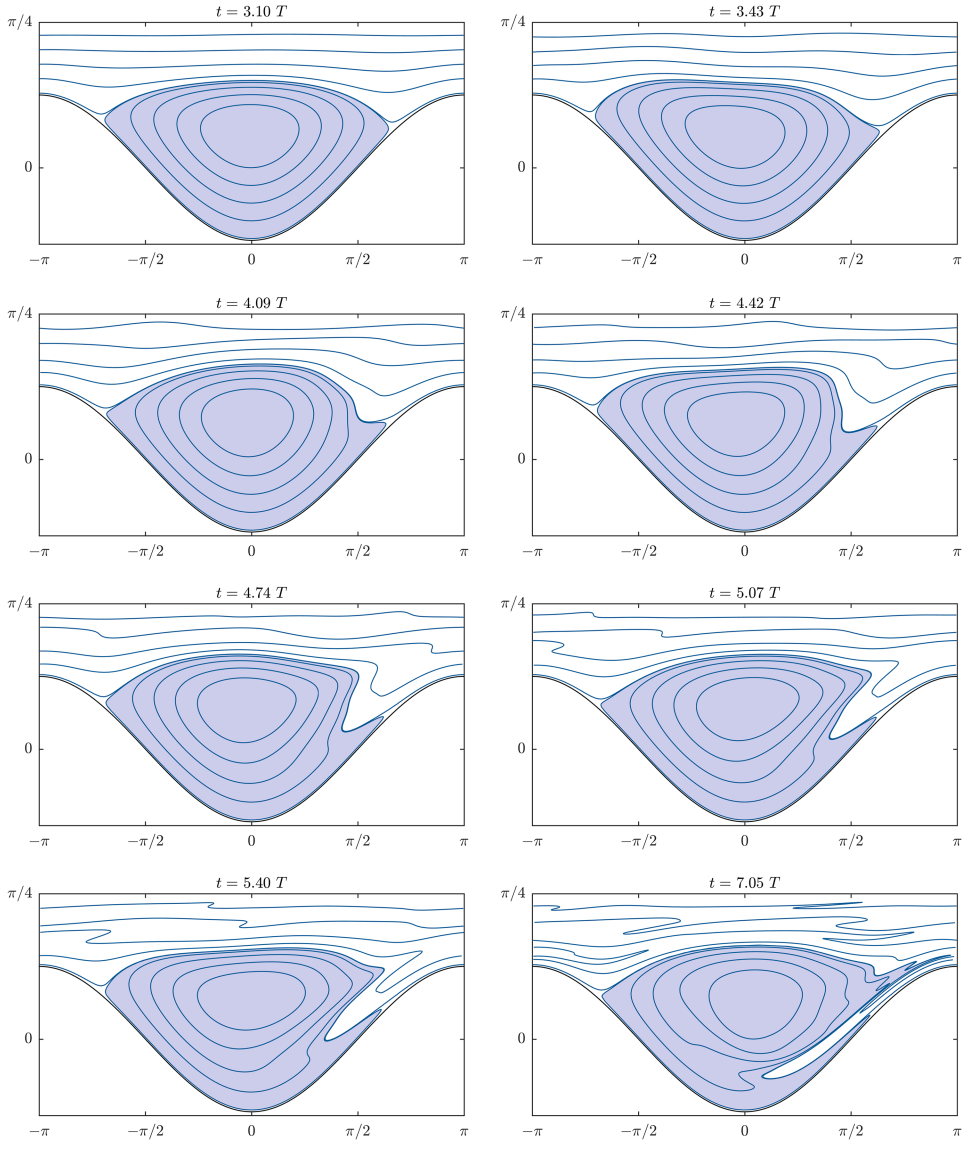

FIG. 8. Sweep lines at different times for the case: $h_0 = \pi/4$, $a = \pi/8$, $h_1 = 0.09$, $\mathrm{Re} = 1$; the shaded area represents the particle distribution at successive times, that was initially confined within the steady-state closed eddy (upper, top left-hand image) at the onset of the unsteady behaviour. Mass transfer takes place between the eddy region and the bulk flow and vice versa.

V. CONCLUSIONS AND OUTLOOK

A principal element of the complex variable method, namely, the reduction of the respective flow to two analytic functions $g_0(\xi)$, $g_1(\xi)$, cannot be maintained as soon as inertia becomes relevant, as clearly indicated by Eq. (5). Accordingly, the first integral of the Navier-Stokes equations, as developed in the present work, does not represent a generalisation of the complex variable method itself, but rather provides an extended nonlinear and unsteady equation set for the complex potential χ which reduces to a simple bianalytic equation and therefore to the Goursat representation in the case of inertial effects being absent. Although much of the analysis based on the holomorphic character of $g_0(\xi)$ and $g_1(\xi)$ is not applicable for the present extension, the first integral features at least a set of field equations, the order of which is reduced by one in comparison to the original Navier-Stokes equations. The first integral is a set of second order PDEs, whereas the original Navier-Stokes equations are

of third order when expressed in terms of the stream function; a fact which is beneficial from both an analytical and a numerical viewpoint. Accordingly, based on the field equations derived, the subsequent development of new semi-analytical and numerical solution methods, suited to complex flow geometries, appears to a worthwhile pursuit. In particular, these could prove very informative with regard to the internal structure of flows, for example, in relation to eddy genesis and the dynamics of the same, by enabling quick identification of relevant areas in a parameter space which would benefit from complementary high-fidelity numerical solutions of the full Navier-Stokes equations themselves. A three-dimensional generalisation of the methodology can be found in the work of Scholle *et al.*,[36] and an alternative approach for a first integral based on the Clebsch transformation was provided by Scholle and Marner.[37,38]

The capabilities of the method have been demonstrated for the unsteady Couette flow in a channel bounded by two sinusoidally corrugated surfaces, via both analytical and numerical means. For the analytical approach, a generalised Goursat form with a third holomorphic function has been established for the stream function, which more generally can be written in the form $\psi = \Re\left[g_0(\xi) + \bar{\xi} g_1(\xi) + \mathrm{Re}\,\bar{\xi}^2 g_2(\xi)\right]$. We note that although this elegant extension of the classical complex variable method is not generally applicable, it can at least be applied to flow problems with negligible nonlinear inertial effects and small Reynolds numbers taking into account the remaining unsteady effects. The asymptotic analysis reveals a time-dependent eddy structure invoking a material exchange, a topical subject of research in relation to coating and film flows. Via numerical studies, based on implicit Crank-Nicolson time discretization in combination with a weak Galerkin finite element formulation, this material exchange has been revealed in detail by visualisation of sweep lines, showing the associated flow structure via a sequence of snap-shots of the ensuing motion. Future studies are planned, which will include the nonlinear inertial terms in the field equations and utilise the approach to explore free surface film flows making use of the elegant reformulation (23) and (27) of the kinematic and dynamic boundary conditions in order to find solutions for solitary surface waves and, finally, to investigate the "turnstile lobe" effect in more detail.

Analysis of the stability of steady-state base flows, subjected to a small disturbance away from equilibrium, is a second attractive research area for application of the field equations (16) and (17). Since they are in complex form they represent a suitable mathematical framework from which to calculate the time evolution of small wave-like perturbations; in combination with the complex form (27) of the dynamic boundary condition, the onset of surface waves in film flows[21] may be explored.

ACKNOWLEDGMENTS

F.M. acknowledges the financial support from the Thomas Gessmann-Stiftung for his doctoral project. M.S. and F.M. acknowledge the support from the DFG (Deutsche Forschungsgemeinschaft), No. SCHO767/6-1.

APPENDIX A: GENERAL CONSIDERATIONS FOR SMALL REYNOLDS NUMBERS

Note that in two dimensions the vorticity ω is given by $2\omega = \Delta\Psi$, and the corresponding evolution equation for ω, the vortex transport equation, is obtained from the imaginary part of (17), by applying the Laplacian $\Delta = 4\partial^2/\partial\xi\partial\bar{\xi}$, as

$$\mathrm{Re}\frac{\partial\omega}{\partial t} - \Delta\omega = -\frac{1}{2}\Delta^2\Im\chi\,, \tag{A1}$$

while taking the derivative of (16) with respect to ξ twice leads to

$$\Delta^2\chi = -\frac{\mathrm{Re}}{2}\frac{\partial^2 u^2}{\partial\xi^2}\,. \tag{A2}$$

The Reynolds number appears in both of the above equations but with a different physical meaning: in Eq. (A2) inertia is present by accounting for quadratic terms, whereas in Eq. (A1) it is related to the unsteady character of the flow.

Assuming that inertia can be neglected due to physical reasoning while retaining the unsteady character of the flow leads to the following simplified vortex transport equation:

$$\mathrm{Re}\frac{\partial\omega}{\partial t} - \Delta\omega = 0\,. \tag{A3}$$

By taking the time derivative of (A3), multiplying the result with Re, and utilising (A3) again gives

$$0 = \mathrm{Re}^2\frac{\partial^2\omega}{\partial t^2} - \Delta\left[\mathrm{Re}\frac{\partial\omega}{\partial t}\right] = \mathrm{Re}^2\frac{\partial^2\omega}{\partial t^2} - \Delta^2\omega\,. \tag{A4}$$

Finally, noting that $\Delta^2\omega = \mathcal{O}\left(\mathrm{Re}^2\right)$ for small Reynolds numbers, and remembering that $2\omega = \Delta\Psi$, leads to

$$\Delta^3\Psi = \mathcal{O}\left(\mathrm{Re}^2\right)\,. \tag{A5}$$

APPENDIX B: FOURIER DISCRETIZATION

1. Base flow: Steady Stokes flow ($h_1 = 0$)

By inserting the series representation (57) and (58) into condition (51) at the upper corrugated surface, it follows that

$$2h_0B\delta_{0n} + \exp(-nh_0)\left[(1-2nh_0)\,Q_n - 2nR_n\right] + \exp(-nh_0)\bar{Q}_{-n} = \delta_{0n}\,. \tag{B1}$$

For $n = 0$ the constant B can be expressed in terms of Q_0 via

$$B = \frac{1}{2h_0}\left[1 - 2\Re Q_0\right]\,, \tag{B2}$$

while for $n > 0$, the negative-indexed Q-coefficients can be expressed in terms of their positive-indexed counterparts,

$$\bar{Q}_{-n} = \exp(-2nh_0)\left[2nR_n - (1-2nh_0)\,Q_n\right]\,. \tag{B3}$$

For the case $n < 0$ use is made of the complex conjugate of the equations and the substitution $n \to -n$, leading finally to

$$\bar{R}_{-n} = -\exp(-2nh_0)\left[(1+2nh_0)\,R_n + 2nh_0^2Q_n\right]\,, \tag{B4}$$

enabling, as above, the negative-indexed R-coefficients to be expressed in terms of their positive-indexed counterparts.

Next, the series representation (57) and (58) is applied to boundary condition (49) related to the lower corrugated surface and considering Equations (B2)–(B4). Furthermore the gauging condition $\Im Q_0 = 0$ is added to the set of equations, and the Fourier decomposition,[39]

$$\exp\left(ka\cos x\right) = \sum_{n=-\infty}^{+\infty}\mathrm{I}_n(ka)\exp(\mathrm{i}nx)\,, \tag{B5}$$

is used with I_n being the modified Bessel functions of order n. Finally, a set of linear algebraic equations follow,

$$\begin{aligned}\sum_{k=0}^{\infty}\Bigg\{&4k^2\frac{\mathrm{I}^{(1)}_{n-k} - h_0\mathrm{I}^{(0)}_{n-k}}{\exp(2kh_0)}\bar{R}_k - 2k\left[\mathrm{I}^{(0)}_{nk} - \frac{\mathrm{I}^{(0)}_{-n-k}}{\exp(2kh_0)}\right]R_k + \left[\mathrm{I}^{(0)}_{nk} - 2k\mathrm{I}^{(1)}_{nk} - \frac{1-2kh_0}{\exp(2kh_0)}\mathrm{I}^{(0)}_{-n-k}\right]Q_k\\ &+\left[\mathrm{I}^{(0)}_{-nk} - \frac{1-2kh_0+4k^2h_0^2}{\exp(2kh_0)}\mathrm{I}^{(0)}_{n-k} + \frac{2k(1-2kh_0)}{\exp(2kh_0)}\mathrm{I}^{(0)}_{n-k}\right]\bar{Q}_k\Bigg\} = \frac{a}{2h_0}\left[\delta_{1n} + \delta_{-1n}\right]\,,\end{aligned} \tag{B6}$$

where $\mathrm{I}^{(0)}_{nk} := \mathrm{I}_{n-k}(ka)$ and $\mathrm{I}^{(p+1)}_{nk} := -a\left[\mathrm{I}^{(p)}_{n-1\,k} + \mathrm{I}^{(p)}_{n+1\,k}\right]/2$ are used as abbreviations ($p = 0, 1$). Note that in (B6) the index n goes from $-N$ to N.

2. Perturbation

By inserting (53)–(55) in (48), the complex conjugate of the velocity reads

$$\bar{u}_{\mathrm{u}} = \left\{ 2\mathrm{i}\left[r^{+'} + yq^{+'} + \mathrm{Re}\,\frac{y^2}{2}p^{+'} \right] + q^{+} + \overline{q^{-}} + \mathrm{Re}\, y\left[p^{+} + \overline{p^{-}} \right] \right\} \exp(+\mathrm{i}t)$$
$$+ \left\{ 2\mathrm{i}\left[r^{-'} + yq^{-'} + \mathrm{Re}\,\frac{y^2}{2}p^{-'} \right] + q^{-} + \overline{q^{+}} + \mathrm{Re}\, y\left[p^{-} + \overline{p^{+}} \right] \right\} \exp(-\mathrm{i}t)\,.$$

Next, by applying the series representation (57)–(59), the following linear algebraic set of equations is obtained ($n \neq 0$) from the boundary condition (50),

$$\sum_{\substack{k=-N \\ k\neq 0}}^{N} \left\{ \left[\mathrm{I}^{(0)}_{nk} - 2k\mathrm{I}^{(1)}_{nk} \pm \frac{\mathrm{iRe}}{2k}\left(k\mathrm{I}^{(2)}_{nk} - \mathrm{I}^{(1)}_{nk} \right) \right] q^{\pm}_{k} + \left[\mathrm{I}^{(0)}_{-nk} \mp \frac{\mathrm{iRe}}{2k}\mathrm{I}^{(1)}_{-nk} \right] \bar{q}^{\mp}_{k} - 2k\mathrm{I}^{(0)}_{nk} r^{\pm}_{k} \right\}$$
$$- a\mathrm{Re}\,(\delta_{1n} + \delta_{-1n})\, p_0 = 0\,, \tag{B7}$$

for the coefficients $q^{\pm}_{k}, r^{\pm}_{k}$, and p_0. For convenience we take the derivative of (51) with respect to x, implying the identity $\partial\bar{u}_{\mathrm{s}}/\partial\xi = -\partial\bar{u}_{\mathrm{s}}/\partial\bar{\xi}$ at $\xi = x + \mathrm{i}h_0$, in order to simplify the boundary condition (52) together with (47) as follows:

$$\bar{u}_{\mathrm{u}}\,(x + \mathrm{i}h_0, x - \mathrm{i}h_0, t) = -2\mathrm{i}\frac{\partial\bar{u}_{\mathrm{s}}}{\partial\bar{\xi}}\cos(x - t) = 2\left[B - 2\Im Q'_{\mathrm{s}} \right]\cos(x - t)\,. \tag{B8}$$

Applying the series representation (57)–(59) again, the boundary condition (52) implies the following linear algebraic set of equations ($n \neq 0$):

$$\frac{\left[1 - 2nh_0 \pm \frac{\mathrm{i}h_0\mathrm{Re}}{2n}\,(nh_0 - 1) \right] q^{\pm}_{n} - 2nr^{\pm}_{n}}{\exp(nh_0)} + \exp(nh_0)\left[1 \pm \frac{\mathrm{i}h_0\mathrm{Re}}{2n} \right]\bar{q}^{\mp}_{-n} = b^{\pm}_{n}\,, \tag{B9}$$

$$2h_0\mathrm{Re}\; p_0 = b^{+}_{0}\,, \tag{B10}$$

for the coefficients $q^{\pm}_{k}, r^{\pm}_{k}$, and p_0, where the inhomogeneity $b^{\pm}_{n}$ is calculated according to

$$b^{\pm}_{n} := B\delta_{\mp 1\, n} - \frac{1}{\pi}\int_{-\pi}^{+\pi} \Im Q'_{\mathrm{s}}\,(x + \mathrm{i}h_0)\exp\left(-\mathrm{i}[n \pm 1]x\right)\mathrm{d}x\,,$$

from the coefficient B and the function Q_{s} of the base solution.

[1] N. I. Muskhelishvili, *Some Basic Problems of the Mathematical Theory of Elasticity* (Noordhoff, Groningen, 1953).
[2] S. G. Mikhlin, *Integral Equations and Their Applications to Certain Problems in Mechanics, Mathematical Physics and Technology* (Pergamon Press, New York, 1957).
[3] V. D. Didenko and J. Helsing, "Stability of the Nyström method for the Sherman–Lauricella equation," SIAM J. Numer. Anal. **49**, 1127–1148 (2011).
[4] L. Greengard, M. C. Kropinski, and A. Mayo, "Integral equation methods for Stokes flow and isotropic elasticity in the plane," J. Comput. Phys. **125**, 403–414 (1996).
[5] M. Scholle, "Creeping Couette flow over an undulated plate," Arch. Appl. Mech. **73**, 823–840 (2004).
[6] C. J. Coleman, "On the use of complex variables in the analysis of flows of an elastic fluid," J. Non-Newtonian Fluid Mech. **15**, 227–238 (1984).
[7] A. Karageorghis and G. Fairweather, "The method of fundamental solutions for the numerical solution of the biharmonic equation," J. Comput. Phys. **69**, 434–459 (1987).
[8] C. Pozrikidis, *Boundary Integral and Singularity Methods for Linearized Viscous Flow* (Cambridge University Press, 1992).
[9] R. H. Chan, T. K. DeLillo, and M. A. Horn, "The numerical solution of the biharmonic equation by conformal mapping," SIAM J. Sci. Comput. **18**, 1571–1582 (1997).
[10] H. Ockendon and J. R. Ockendon, *Viscous Flow*, Cambridge Texts in Applied Mathematics (Cambridge University Press, 1995).
[11] S. Richardson, "Two-dimensional slow viscous flows with time-dependent free boundaries driven by surface tension," Eur. J. Appl. Math. **3**, 193–207 (1992).
[12] S. Tanveer and G. L. Vasconcelos, "Time-evolving bubbles in two dimensional Stokes flow," J. Fluid Mech. **301**, 325–344 (1995).
[13] S. Howison, "Complex variable methods in Hele-Shaw moving boundary problems," Eur. J. Appl. Math. **3**, 209–224 (1992).
[14] M. Scholle, A. Wierschem, and N. Aksel, "Creeping films with vortices over strongly undulated bottoms," Acta Mech. **168**, 167–193 (2004).

[15] M. Scholle, A. Haas, N. Aksel, M. C. T. Wilson, H. M. Thompson, and P. H. Gaskell, "Competing geometric and inertial effects on local flow structure in thick gravity-driven fluid films," Phys. Fluids **20**, 123101 (2008).
[16] F. Marner, P. H. Gaskell, and M. Scholle, "On a potential-velocity formulation of Navier-Stokes equations," Phys. Mesomech. **17**, 341–348 (2014).
[17] L. K. Antanovskii, "Boundary integral equations in quasi-steady problems of capillary fluid mechanics. Part 2: Application of the stress-stream function," Meccanica **26**(2-3), 59–65 (1991).
[18] M. Scholle, A. Haas, and P. H. Gaskell, "A first integral of Navier-Stokes equations and its applications," Proc. R. Soc. A **467**, 127–143 (2011).
[19] K. B. Ranger, "Parametrization of general solutions for the Navier-Stokes equations," Q. Appl. Math. **52**, 335–341 (1994).
[20] H. Goldstein, C. P. Poole, and J. L. Safko, *Klassische Mechanik* (Wiley-VCH, 2006).
[21] M. Schörner, D. Reck, and N. Aksel, "Does the topography's specific shape matter in general for the stability of film flows?," Phys. Fluids **27**, 042103 (2015).
[22] A. E. Malevich, V. V. Mityushev, and P. M. Adler, "Couette flow in channels with wavy walls," Acta Mech. **197**, 247–283 (2008).
[23] Y. Y. Trifonov, "Viscous liquid film flows over a periodic surface," Int. J. Multiphase Flow **24**, 1139–1161 (1999).
[24] S. F. Kistler and P. M. Schweizer, *Liquid Film Coating* (Chapman Hall, 1997), Vol. 185.
[25] M. Scholle, A. Haas, N. Aksel, M. C. T. Wilson, H. M. Thompson, and P. H. Gaskell, "Eddy genesis and manipulation in plane laminar shear flow," Phys. Fluids **21**, 073602 (2009).
[26] B. Szulczewska, I. Zbicinski, and A. Gorak, "Liquid flow on structured packing: CFD simulation and experimental study," Chem. Eng. Technol. **26**, 580–584 (2003).
[27] A. Wierschem and N. Aksel, "Influence of inertia on eddies created in films creeping over strongly undulated substrates," Phys. Fluids **16**, 4566–4574 (2004).
[28] P. H. Gaskell, P. K. Jimack, M. Sellier, H. M. Thompson, and M. C. T. Wilson, "Gravity-driven flow of continuous thin liquid films on non-porous substrates with topography," J. Fluid Mech. **509**, 253–280 (2004).
[29] D. R. J. Slade, "Gravity-driven thin liquid films: Rivulets and flow dynamics," Ph.D. thesis, University of Leeds, 2013.
[30] S. Veremieiev, H. M. Thompson, and P. H. Gaskell, "Free-surface film flow over topography: Full three-dimensional finite element solutions," Comput. Fluids **122**, 66–82 (2015).
[31] M. Horner, G. Metcalfe, S. Wiggins, and J. Ottino, "Transport enhancement mechanisms in open cavities," J. Fluid Mech. **452**, 199–229 (2002).
[32] M. C. T. Wilson, J. L. Summers, N. Kapur, and P. H. Gaskell, "Stirring and transport enhancement in a continuously modulated free-surface flow," J. Fluid Mech. **565**, 319–351 (2006).
[33] F. M. Esquivelzeta-Rabell, B. Figueroa-Espinoza, D. Legendre, and P. Salles, "A note on the onset of recirculation in a 2D Couette flow over a wavy bottom," Phys. Fluids **27**, 014108 (2015).
[34] M. Scholle, "Hydrodynamical modelling of lubricant friction between rough surfaces," Tribol. Int. **40**, 1004–1011 (2007).
[35] T. Tezduyar, R. Glowinski, and J. Liou, "Petrov-Galerkin methods on multiply connected domains for the vorticity-stream function formulation of the incompressible Navier-Stokes equations," Int. J. Numer. Methods Fluids **8**, 1269–1290 (1988).
[36] M. Scholle, P. H. Gaskell, and F. Marner, "Exact integration of the unsteady incompressible Navier-Stokes equations utilising tensor potentials," J. Math. Phys. (unpublished).
[37] M. Scholle and F. Marner, "A generalized Clebsch transformation leading to a first integral of Navier-Stokes equations," Phys. Lett. A **380**, 3258–3261 (2016).
[38] M. Scholle and F. Marner, "A non-conventional discontinuous Lagrangian for viscous flow," R. Soc. Open Sci. **4**, 160447 (2017).
[39] M. Abramowitz and I. A. Stegun, *Handbook of Mathematical Functions with Formulas, Graphs, and Mathematical Tables*, National Bureau of Standards, Applied Mathematics Series Vol. 55 (Dover Publications, 1970).